Development of a Novel Gamma Camera Based on Deposited Energy Distribution*

Lin Song,[1] Hao-Tian Qi,[1] and Li-Hua Zhu[1,†]

[1] *School of Physics, Beihang University, Beijing 100191, China*

Radioactive substances have a wide range of applications in medical diagnosis, industrial irradiation, scientific research and education, environmental monitoring and other fields, so rapid and efficient monitoring methods are increasingly important. The existing monitoring means are mainly divided into two categories: counting equipment and gamma camera. The counting equipment can only give information such as counting and intensity, but cannot give location information; gamma cameras either use bulky collimators (such as various devices based on coded hole imaging) or require high-performance detectors and complex image reconstruction algorithms (such as Compton cameras), which are difficult to make portable and mass-promote. In this work, a new gamma camera based on the deposition energy distribution was developed. The main part of the device is composed of a $LaBr_3$ (Ce) scintillator array coupled with a SiPM array, which does not require a collimator and uses a TOFPET2-type ASIC chip for data acquisition. The imaging sensitivity, imaging accuracy and other parameters of the device were determined by using the Cs-137 source to simulate the hot spots in the actual situation. Experiments show that the higher the number of accumulated events, the higher the reconstruction accuracy of the device, and when the number of events reach 10,000, The device can operate stably, with a maximum deviation of less than 2.5°. The device has an imaging field of view of 4π, but the reconstruction accuracy will be different when the hot spot is in different directions of the detector, and the maximum deviation can be less than 2.5° in most cases by rotating the detector. As a result, the device can be applied to the monitoring of radioactive source hotspots in nuclear safety applications.

Keywords: Deposited Energy Distribution; Scintillator Array; Gamma Camera; 4π field of view

I. INTRODUCTION

With the continuous development and application of nuclear science and technology, radioactive materials are playing an increasingly important role in various fields such as industrial irradiation, nuclear power generation, medical imaging, and scientific research and education [1, 2]. In the event of the loss or leakage of radioactive materials, the ability to quickly and accurately locate the radioactive source is crucial for minimizing harm to the public and search personnel, as well as for preventing public panic. To achieve the monitoring and management of radioactive materials, the commonly used monitoring equipment can be currently classified to two types: counting devices and gamma cameras [3–6].

Counting devices, such as Geiger-Muller counters, only provide information on such as counts and intensity, and can only roughly judge whether the radiation source is close or far based on the change in the number of counts, without providing location information [7]. Of course, multiple counting devices can be used simultaneously to form a system for position determination, but this method has a small imaging field of view, low accuracy, and is only applicable to single radiation sources. Using gamma cameras to determine the location of radiation sources is a more effective method [8]. The commonly used gamma cameras are generally divided into two major categories: with and without mechanical collimation [9]. Mechanical collimation mainly uses various types of coded plates, which improve the accuracy of position reconstruction but greatly reduce sensitivity and field of view. Moreover, coded plates are often built with high-density metals such as lead and tungsten, which greatly increase the carrying weight and are not suitable as portable devices. Gamma cameras without mechanical collimation mainly refer to Compton cameras [10–12], which can achieve few-event imaging and 4π field of view. However, Compton cameras are expensive and complex in structure. The imaging accuracy of Compton cameras in actual use is lower than that of gamma cameras using coded plates. Some commercial Compton camera products have been developed internationally, such as H3D in the United States [13] and ASTROCAM in the Japan Aerospace Research Institute (ISAS) [14]. The research on Compton camera technology in China started relatively late, but it has made significant progress in recent years. Guo Xiaofeng et al. have carried out research on the Compton Camera composed of CZT detectors based on Geant4 [15]. Liu Yilin of Tsinghua University have built Compton cameras based on 4×4 pixel 3-D CZT detectors [16]. Song Lin of Beihang University have developed a Compton camera based on a monolithic GAGG (Gadolinium Aluminum Gallium Garnet) crystal [17].Currently, there are very few Compton camera products in China that have been independently developed and can be launched into market applications. Commercial Compton cameras need to be characterized by high resolution, low cost, and miniaturization, which are technically difficult and expensive to develop. In addition, some 4π imaging devices of other configurations have also been reported [18–20].

We propose a novel gamma imaging device without collimators, which can image radiation sources in a 4π field of view using a scintillator array. The device is based on a LaBr3(Ce) scintillator array. When the array is exposed to radiation sources, a specific energy deposit distribution will form depending on the following factors: the shielding relationship between each crystal, the penetration distance of the

* Supported by the National Natural Science Foundation of China (Grant Nos. U1867210, 12325506, 1922501)

† Corresponding author, Li-Hua Zhu, School of Physics, Beihang University, 13520056359, zhulh@buaa.edu.cn.

ray beam in the crystal, and the angular relationship between the radiation source and the crystals. This distribution is sensitive to the position of the radiation source. Therefore, the position of the radiation source can be determined from different deposited energy distributions measured with the array. In this study, we built a prototype gamma camera based on the deposited energy distribution and tested its performance.

II. THE EXPERIMENTAL EQUIPMENT

The prototype gamma camera is a $LaBr_3(Ce)$ scintillator array (Fig.1(left)), which consists of a set of $LaBr_3(Ce)$ scintillators coupled with two 8×8 arrays of SiPMs. The scintillator array contains an 8×8 grid of $LaBr_3(Ce)$ scintillators, each with dimensions of $6 \times 6 \times 50$ mm^3 polished on all six faces, and wrapped with a ESR film with 0.067 mm in thickness on four sides as a reflective layer, excluding the two end faces. Due to the hygroscopic of $LaBr_3(Ce)$, the array is encased in an aluminum shell with 2 mm in thickness on four sides, with the remaining two faces serving as the optical output, sealed with quartz glass of dimensions $52 \times 52 \times 1.5$ mm^3. The two optical output faces of the encapsulated scintillator array are coupled with two SiPM arrays through the air, with each SiPM array containing an 8x8 grid of MicroFJ-60035 type SiPMs, each with a sensitive area of 6.07×6.07 mm^2. The readout system employs two TOF-PET2 type ASIC chips[21], each capable of accommodating 64 channels, with each channel providing functions such as leading edge discriminator (LED), time-to-digital conversion (TDC), and charge integration (QDC). During the experiment, the ASIC chips record the experimental information for each channel, including the timestamp from the leading edge timing, the amplitude from the QDC, and the channel number. The recorded experimental data are packaged by the motherboard and sent to the upper computer, exported in ROOT format for subsequent processing.

Fig.1 (right) shows the experimental setup used in this study. The main body consists of two large protractors. By changing the position of the source on the vertical protractor, different θ is obtained. The detector is rotated to obtain different ϕ. A 2 μCi Cs-137 collimated source was used in the experiment, with the source placed by 30 cm away from the detector.

III. IMAGING PRINCIPLE

Fig.2 is a schematic diagram of the principle of the gamma-ray imaging device developed in this study. The detector used in this study is an 8×8 array, but only a 4×4 array is shown here for demonstration purposes. The red dot represents a radioactive source at an arbitrary position in space. In actual detection, the radioactive source may have a shape, but the distance between the source and the detector is usually quite large, allowing it to be approximated as a point source. Therefore, in subsequent experiments, a point source is used to simulate the actual detection scenario. The direction of the radioactive source is determined by (θ,ϕ), when changing (θ,ϕ) the energy deposition distribution is changed accordingly . The deposited energy here refers to the total energy deposited within a crystal during the measurement period. There is no need to distinguish whether the interaction type is Compton scattering, photoelectric effect, or other types. At the same time, this experiment does not consider the interaction positions of γ rays within the crystal. Changes in the energy deposition distribution are mainly due to the following three situations.

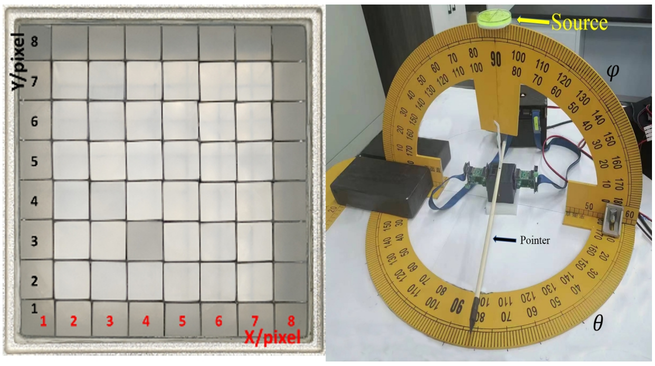

Fig. 1. $LaBr_3(Ce)$ scintillator array (left). Experimental measurement setup (right)

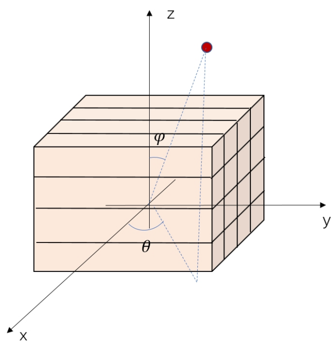

Fig. 2. Schematic diagram of the principle of γ-ray imaging equipment

Situation 1): The shielding relationship between crystals changes, for example: θ=0° and ϕ changes. Fig.3(left) shows the side view (x-z plane) of the detector when this change occurs. During the change in ϕ, the mutual shielding situation between crystals changes significantly, leading to a noticeable change in the energy deposition distribution.

Situation 2): The penetration distance of the ray beam within the crystal changes, for example: ϕ=90° and θ changes from 0° to 45°. Fig.3(middle) shows the top view(x-y plane) of the detector when this change occurs. During the change in θ, the mutual shielding situation between crystals remains essentially unchanged, but the penetration distance within each crystal changes, leading to a change in the energy deposition distribution. The figure only illustrates the case where θ changes from 0° to 45°. For the case where θ changes from

0° to -45° and other symmetric positions, the situation is similar.

Situation 3): The angular relationship between the radioactive source and the crystal face changes, for example: ϕ=90° and θ changes from 45° to 90°. Fig.3(right) shows the top view of the detector when this change occurs. The radioactive source has an angular relationship with each crystal face, and 64 crystals form an angular distribution, which changes when the position of the radioactive source changes. The figure only illustrates the case where θ changes from 45° to 90°. For the case where θ changes from 90° to 135° and other symmetric positions, the situation is similar.

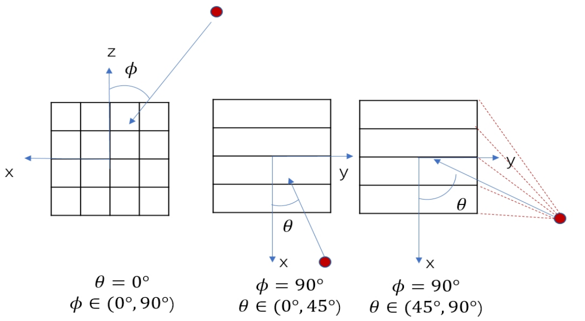

Fig. 3. Schematic diagram of the three main conditions that affect the distribution of deposited energy

The above special positions explain the reasons for the changes in the energy deposition distribution caused by the change in the position of the radioactive source. In reality, when the position of the radioactive source changes, the three situations often change simultaneously, and which situation plays a dominant role determines the imaging accuracy at that position. Of course, in addition to the above three situations, the geometric shape of the detector housing, the inhomogeneity of the detector crystals, the packaging layer of the $LaBr_3$(Ce) crystals, and the quartz window, among other factors, will also affect the energy deposition distribution. However, these factors either have a relatively small impact or are not sensitive to changes in the position of the radioactive source, and this study does not discuss them in more detail.

IV. ALGORITHM

After a radioactive source is fixed at a position (θ,ϕ) for a sufficient amount of time, the energy deposition distribution in the detector stabilizes. If the position of the radioactive source changes, the energy deposition distribution in the detector also changes accordingly. This is the theoretical basis for the development of the equipment in this project.Considering that the energy deposition distribution within the detector is influenced by many factors, it is difficult to represent it with a simple formula. In this experiment, a database lookup method is used for position reconstruction. First, we experimental record the energy deposition distribution within the detector when the radioactive source is at angles such as (0°, 0°), (0°, 5°)...(0°, 90°), (5°, 0°), (5°, 5°)...(5°, 90°), and establish a database that corresponds one-by-one between (θ, ϕ) and the energy deposition distribution. When actual detection is performed, an energy deposition distribution is obtained. This distribution is compared with the distributions in the database to find the most similar (θ, ϕ), which is then considered as the reconstructed direction of the radioactive source.Obviously, the larger the database, in other words the smaller the step size of (θ, ϕ), the more precise the reconstruction accuracy. However, the smaller the step size, the greater the workload required to build the database. If the future application of this imaging device requires a ignificant amount of time to build the database, it is clearly unreasonable.

We use interpolation to expand a database, thus improving the reconstruction accuracy while avoiding the time cost associated with building a large database. In Fig.4(left), the red points represent four experimental measurement points, with a relatively large angular interval between them, and the blue point represents the arbitrary position which isn't experimental measurement point. In Fig.4(right), $E_i(\theta, \phi)$ represents the energy deposited in the i(0,1,...,63) crystal of the detector per unit time when the radioactive source is in the (θ, ϕ) direction. $E_i(\theta, \phi + \Delta\phi)$, $E_i(\theta + \Delta\theta, \phi)$ represent the energy deposited in the i(0,1,...,63) crystal of the detector per unit time after the (θ, ϕ) changes by step-size $\Delta\phi$, $\Delta\theta$, where $\Delta\phi$, $\Delta\theta$ are relatively large values. $E_i(\theta, \phi)$, $E_i(\theta, \phi + \Delta\phi)$, $E_i(\theta + \Delta\theta, \phi)$, $E_i(\theta + \Delta\theta, \phi + \Delta\phi)$ are all known data obtained from experimental measurements. Using the Eq.(1), the value of $E_i(\theta^{'}, \phi^{'})$ is obtained. The interpolated $E_i(\theta^{'}, \phi^{'})$ can have a very small step size difference from $E_i(\theta, \phi)$. In this way, we have expanded the large step size database based on experimental measurement data such as $E_i(\theta, \phi)$ into a small step size database. Using the expanded database for reconstruction can significantly improve the reconstruction accuracy.

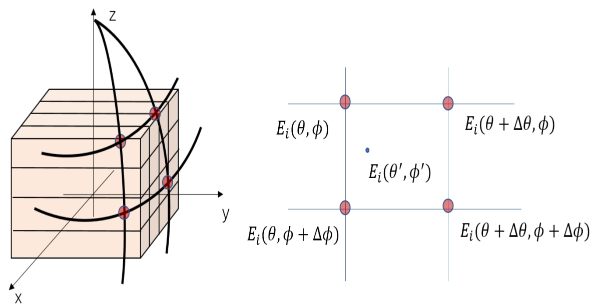

Fig. 4. Left: the red dots represent the experimental measurement points with relatively large angular intervals, while the blue dots represent arbitrary position points; Right: Schematic diagram of interpolation.

$$E_i(\theta^{'},\phi^{'}) = (1-u)(1-v)E_i(\theta,\phi) + u(1-v)E_i(\theta,\phi+\Delta\phi) + (1-u)vE_i(\theta+\Delta\theta,\phi) + uvE_i(\theta+\Delta\theta,\phi+\Delta\phi) \quad (1)$$

While u=($\phi^{'}$-ϕ)/$\Delta\phi$, v=($\theta^{'}$-θ)/$\Delta\theta$.

V. EXPERIMENT

Based on the aforementioned imaging principles and reconstruction algorithms, it is necessary to experimentally determine a set of large step-size databases as a benchmark, which will then be expanded into small step-size databases using interpolation methods. The large step-size database established in this experiment is $\Delta\phi$ = 5° for ϕ ϵ (0°, 90°)and $\Delta\theta$ = 5° for θ ϵ (0°, 90°). This portion is equivalent to one-eighth of the entire 4π space. Due to symmetry, the other parts are consistent with the measured parts, hence there is no need to measure the entire 4π space.

The database is expanded into a small step-size database using interpolation, with this study expanding the database to a step-size of 0.2°.After establishing the database, we measured the energy deposition distributions for some positions (θ, ϕ) not within the large step-size database and performed position reconstruction to verify the performance of our detector. These tested (θ, ϕ) positions include: Experiment 1: θ = 0°,ϕ ϵ (10°,90°)with a step-size of $\Delta\phi$ = 2°, to illustrate the impact of situation one on (θ, ϕ) as described in the imaging principles; Experiment 2: ϕ = 90°, θ ϵ (10°,80°)with a step-size of $\Delta\theta$ = 2°, to illustrate the impact of situations 2) and 3) on (θ, ϕ) as described in the imaging principles; Experiment 3: ϕ = θ,ϕ ϵ (10°,80°) ,θ ϵ (10°,80°), with a step-size of $\Delta\phi$ = $\Delta\theta$ = 1°, A set of (θ, ϕ) along the diagonal is selected to represent the (θ, ϕ) in the entire space; Experiment 4: To enhance the imaging performance of the detector, the detector array was rotated. The reasons and effects of this operation will be detailed in the following text; Experiment 5: Multi-point source imaging test.

VI. EXPERIMENTAL RESULTS

A. Detector Performance Study

Before conducting position reconstruction tests, the basic performance of the detector array used in this study was tested. An 8 × 8 $LaBr_3$(Ce) scintillator array was used in this study, and the detector array was energy-calibrated using Cs-137 sources. Fig.5 shows the energy spectra of the 64 crystals using Cs-137 sources, with energy resolutions varying in the range of (12-19)%@662 keV. For $LaBr_3$(Ce) crystals, this is a relatively poor energy resolution [22]. The reason for such a poor energy resolution is that each crystal has a quartz glass with 2 mm in thickness on the end faces. This quartz glass encapsulates the crystals to prevent deliquescence and serves as a light guide. However, when a γ-ray interacts within a crystal, the scintillation light produced can pass through the quartz glass and cause crosstalk with the scintillation light from adjacent crystals. Experiment has shown that the scintillation photons involved in the crosstalk can even exceed half of the total number of photons produced, resulting in a poor energy resolution for individual crystals. One way to improve this phenomenon is to reduce the thickness of the quartz glass, but a quartz glass that is too thin will not be effective in preventing the deliquescence of the $LaBr_3$(Ce) crystals, and it also requires very high manufacturing precision.

In Fig.5, the lower limit of the energy spectrum is set at 400 ch, 400 ch is not an energy value but a parameter of the detector itself. The reason for setting the lower limit is the existence of crosstalk, which results in a large number of small signals. Without setting the lower limit, the counting rate would be extremely high. In Fig.5, the full-energy peaks of some crystals are not obvious. This is because the radioactive source was placed on one side of the detector during the experiment, so the crystals on the side farther from the radioactive source received fewer full-energy peak events. In this experiment, the energy resolution of the 64 crystals was determined by changing the position of the radioactive source. Fig.5 only shows one-time experimental result . Meanwhile, Fig.5 well illustrates an issue that there is a certain response relationship between the 64-channel energy spectra and the position of the radioactive source. This is also the inspiration for using the deposited energy distribution for radioactive source position reconstruction.

In this experiment, the end face size of each crystal in the detector is 6 × 6 mm^2, and the degree of pixelation is not very high. Fig.6 shows the deposited energy distribution in the detector array when the radioactive source is incident along the direction of the red arrow. This indicates that the deposited energy distribution exists at this level of pixelation, which forms the basis for subsequent work. Of course, the higher the degree of pixelation, the more obvious the distribution will be, and the higher the reconstruction accuracy will be. This is an important direction for future equipment optimization. In this experiment, the total deposited energy distribution was used for reconstruction instead of the energy spectrum distribution. The reason is that the reconstruction algorithm based on the total deposited energy distribution is simpler, and the imaging accuracy is sufficient. In the future, reconstruction algorithms based on the energy spectrum distribution could be developed, which may offer higher sensitivity and accuracy.

B. The impact of situation 1) on reconstruction accuracy

In the experiment, the radiation source was placed at positions where θ = 0° and ϕ ϵ (10°,90°) with a step size $\Delta\phi$ = 2°. A sufficient number of γ-ray interactions with the detector (hereinafter referred to as events) are required to obtain a stable energy deposition distribution. In this experiment, three modes were adopted: the deposited energy distribution of 1,000 events, the deposited energy distribution

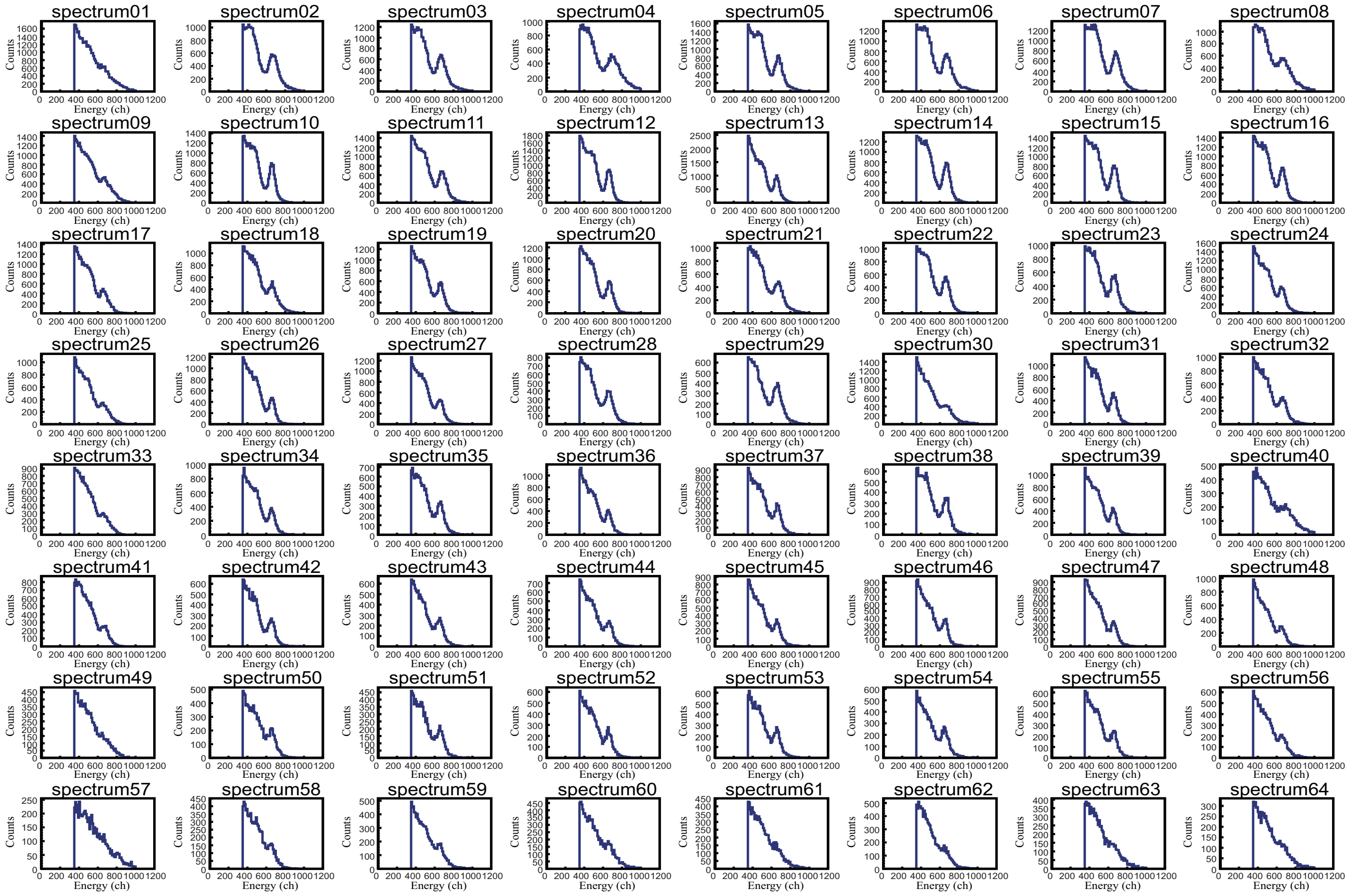

Fig. 5. The energy spectra of 64 crystals using a Cs-137 source. The source is fixed at one position, Due to the different relative positions of each crystal to the source, the energy spectra vary from one another.

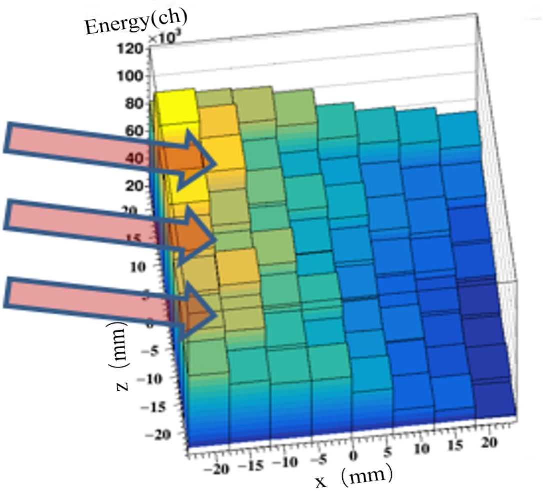

Fig. 6. The distribution of deposited energy in the detector array after γ rays are incident in one direction

of 10,000 events, and the deposited energy distribution of 100,000 events. The 1000 events refer to a total of 1000 events recorded by the radiation source in 64 crystals, not 1000 events recorded within a single crystal, and the same one applies to the other modes. A radioactive source(Cs-137) with an activity of 2 μCi was used in this experiment, placed 30 cm away from the detector, and the measurement time to record 1000 events was approximately 10 s.

Position reconstruction was performed under the three modes, and the results are shown in Fig.7. The horizontal axis ϕ represents the radiation incident direction (0°, ϕ), the vertical axis $\delta\phi$ represents the deviation between the reconstruction result and the actual incident direction (the same meaning applies to $\delta\theta$ in the following text). For 1000 events mode , the maximum deviation is 5.5°, and the average deviation is 4.1°. For 10000 events mode, the maximum deviation is 2.5°, and the average deviation is 1.3°. For 100000 events mode, the maximum deviation is 0.4°, and the average deviation is 0.1°. The experimental step-size is 2°, but average deviation for 1,000 events mode is 4.1° , which indicates that the detector has not yet reached a stable working state when only 1000 events are recorded. For the 100000 events mode, the average deviation of 0.1° is very good, but this requires a measurement time of 1000 seconds, which is not suitable for future practical applications. Fot the 10000 events mode, the average deviation of 1.3° is less than the experimental step-

size, and the imaging time (100 seconds) is also acceptable. Therefore, this imaging mode is chosen for subsequent experiments.

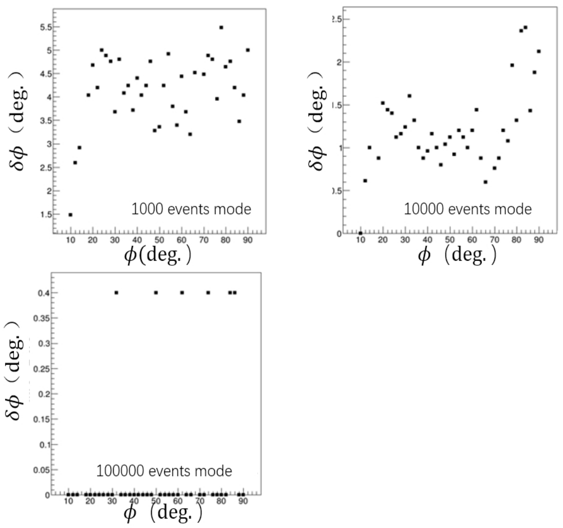

Fig. 7. The reconstruction deviations under three different modes, when the radiation source is placed at positions with θ=0° and ϕ = 10°,12°,14°,...,90°

C. The impact of situation 2) and 3) on reconstruction accuracy

The radiation source was placed at positions with ϕ = 90° and $\theta \in$ (10°,80°) with a step-size $\Delta\theta$ = 2°. When θ < 40°, situation 2) has a greater impact on reconstruction accuracy, and a relatively large maximum deviation of 4° can be obtained. This indicates that when the direction of radiation incidence changes, the change in the penetration distance of the beam within the crystal is small, resulting in an inconspicuous change in the energy deposition distribution. Of course, it could also be due to the severe crosstalk in the array used in this experiment, which fails to respond to these changes. As θ increases, the impact of situation 3) on the energy deposition distribution gradually increases, and the reconstruction accuracy also gradually improves. When θ > 40°, the maximum deviation loss than 2.5°.

D. the reconstruction accuracy at arbitrary positions

It is challenging to reconstruct all directions within the entire 4π space in the experiment. Therefore, we select a set of experimental points to represent the entire 4π space. The incident directions for these experimental points are (10°+n$\Delta\theta$, 80°-n$\Delta\phi$), n = (0, 1, 2...), and $\Delta\theta$, $\Delta\phi$ are the step-sizes. In this experiment $\Delta\theta$ = $\Delta\phi$ = 1°, Fig.9a. Fig.9b and Fig.9c show the reconstruction accuracy of ϕ, θ. When testing experimental points that already exist in the large step-size database, such as points (20°, 70°), (30°, 60°), (35°, 55°) etc.,

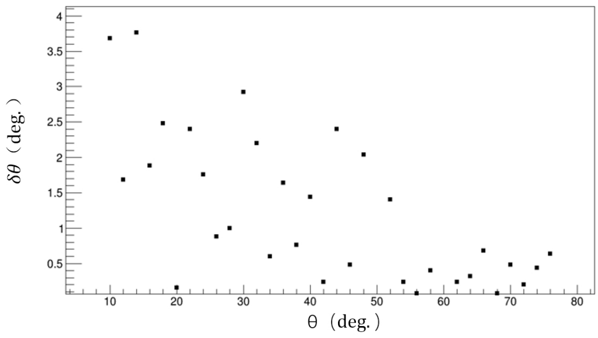

Fig. 8. The reconstruction deviations when the radiation source is located at positions with ϕ = 90° and θ= 10°,12°,14°,...,90°

the reconstruction accuracy is very good, with both ϕ and θ maximum deviation being less than 2°. When testing experimental points that do not exist in the large step-size database, the reconstruction accuracy has a certain relationship with the incident angle, mainly divided into two cases.

The first case is for θ < 40°. When the radiation source is located in those positions, the maximum deviation of ϕ is very small, less than 2°, but the maximum deviation of θ is rather large, even reaching 8°. The reconstruction accuracy of ϕ in this case mainly depends on situation 1) in the imaging principles, where the shielding relationship between crystals causes changes in the energy deposition distribution, which is very sensitive to changes in the radiation source position. The reconstruction accuracy of θ mainly depends on situation 2) in the imaging principles. The poor reconstruction accuracy of θ is also predictable and consistent with the experimental results from the previous section.

The second case is for θ > 40°. When the radiation source is located in this region, the reconstruction accuracies of both ϕ and θ becomes extremely poor. In such cases, the reconstruction accuracy of ϕ and θ mainly depends on situation 3) in the imaging principles, which is the angular distribution of the radiation source relative to the crystal faces. The interpolation method needs to consider the step size when dealing with position reconstruction under situation 3). The premise of the interpolation method is that when the radiation source position changes continuously, the energy deposition in the crystal also changes continuously and monotonically. If the step size is too large and the energy deposition is no longer monotonic, results of the interpolation method will be terrible. To solve this problem, we propose two solutions. The first is to reduce the step-size of the large step-size database; the step size in this experiment is 5°, and it is recommended to reduce the step size to 2°. The second is to rotate the detector to ensure that the radiation source position is always within the θ < 40° position for position reconstruction. When the radiation source position is not in the first part, rotate the detector to bring the radiation source position into the first part. Although the first solution is simple and effective, it greatly increases the cost and is not our preferred solution. This study adopted the scheme of rotating the detector.

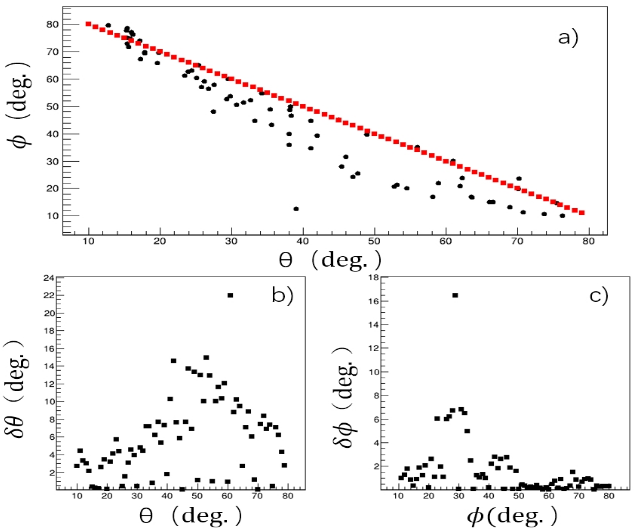

Fig. 9. a: experimental points (red dots) and reconstructed locations (black dots).b: reconstruction accuracy of θ.c: reconstruction accuracy of ϕ

E. Improving Reconstruction Accuracy by Rotating the Detector

In actual measurements, we do not know the position of the radiation source, so it is not possible to directly rotate the detector to ensure that the radiation source falls into the position where $\theta < 40°$. Therefore, a scheme of rotating the detector is adopted here, and Fig.10 illustrates the operating procedure.

In the figure, the blue dot represents a radiation source at an arbitrary position. The first measurement is taken without rotating the detector, resulting in the reconstruction (θ_1, ϕ_1). The detector is then rotated clockwise by 30° for the second measurement, and the reconstruction result is (θ_2, ϕ_2). Finally, the detector is rotated clockwise by 60° for the third measurement, resulting in the reconstruction (θ_3, ϕ_3). The best result among the three measurements is selected as the final measurement outcome. The final reconstruction result is obtained by consulting Table 1.

Using this scheme, position reconstruction is performed for experimental points where $\theta \in (10°,80°)$. The reconstruction results are shown in Fig.11, with the ϕ maximum deviation being less than 2° in most positions. The θ reconstruction accuracy remains poor, which is because under this scheme, the θ reconstruction accuracy always depends on situation 2) in the imaging principles, and situation 2) is not sensitive to the position of the radiation source.

It needs to be explained here that the scheme of rotating the detector can make the maximum deviation of the ϕ less than 2° in the whole imaging range, but the reconstruction accuracy of θ is still very poor, and there are many solutions to solve this problem. Scheme 1:Two sets of detectors are used simultaneously, one for measuring ϕ and the other for measuring θ. Scheme 2: Use only one set of detectors, measure the ϕ first, and then rotate the detector 90° clockwise along the ox axis in Fig.2, the ϕ of the detector after rotation is θ of the detector before rotation, than use the detector after rotation to measure θ. Scheme 3: In this study, the crystal strips of the detector are all arranged in the same direction, we can rotate some of the crystal strips in the whole crystal column to make a cross form, so that the ϕ and θ can be measured at the same time.

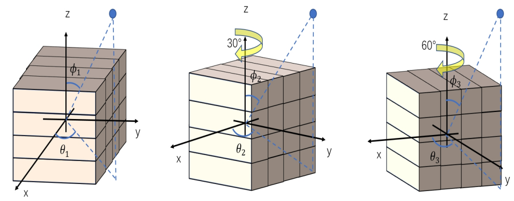

Fig. 10. By rotating the detector, multiple measurements are taken for the same radiation source.

Table 1. Lookup table for the optimal reconstruction results from multiple measurements

three measurement results with the detector rotated (θ_1, ϕ_1), (θ_2, ϕ_2), (θ_3, ϕ_3)	Reconstruction results (θ, ϕ)
only $\theta_1 \in (0°, 30°)$	$\theta = \theta_1$, $\phi = \phi_1$
only $\theta_2 \in (0°, 30°)$	$\theta = \theta_2+30°$, $\phi = \phi_2$
only $\theta_3 \in (0°, 30°)$	$\theta = \theta_3+60°$, $\phi = \phi_3$
$\theta_1 \in (0°, 30°)$ and $\theta_2 \in (0°, 30°)$	$\theta = (\theta_1+\theta_2+30°)/2$ $\phi = (\phi_1 + \phi_2)/2$
$\theta_2 \in (0°, 30°)$ and $\theta_3 \in (0°, 30°)$	$\theta = (\theta_2+30°+\theta_3+60°)/2$ $\phi = (\phi_2 + \phi_3)/2$

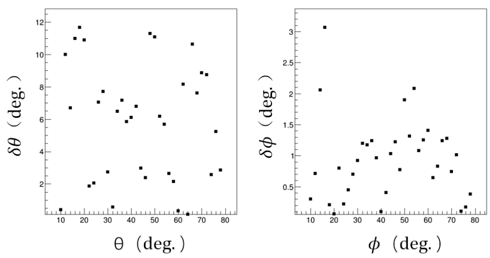

Fig. 11. The reconstruction deviations of θ and ϕ using the scheme of rotating the detector for multiple measurements.

F. Multi-Source Imaging

When there are multiple radiation sources, the deposited energy distribution is equivalent to the superposition of the deposited energy distributions from multiple radiation sources. The deposited energy distributions from multiple radiation sources at different locations are combined and superimposed to obtain some superimposed deposited energy distributions. The obtained deposited energy distributions are compared with the measured deposited energy distributions

to find the most similar situation. In the experiment, two 2 μCi Cs-137 collimated sources were placed at incident angles of (25°, 30°) and (25°, 50°), 30 cm away from the detector. A total of 20,000 events were accumulated and recorded, and position reconstruction was performed using these 20,000 events. Each point in the Fig.12 represents one time reconstruction using 1000 events, and a total of 20 times reconstruction is performed for 20000 events, and the average value of the 20 reconstructions is (21.5°, 32.1°) (22.8°, 49.4°). The reconstruction results have a small deviation in the ϕ direction (< 2.5°) and a slightly larger deviation in the θ direction.

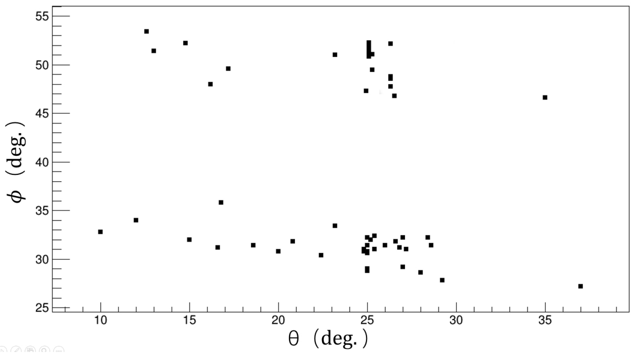

Fig. 12. Multi-source reconstruction

VII. DISCUSSION

In this work, we propose a novel gamma camera based on the deposition energy distribution, which is based on the $LaBr_3$ (Ce) scintillator detector array. When the detector is irradiated by a radioactive source, the deposited energy of the radioactive source in each crystal forms a distribution, which is sensitive to the location of the radioactive source. The concept of using distribution to estimate the position of radiation sources has been used in previous work [23], but most of them use count distributions or interaction position distributions. In this work, we propose a scheme to use the deposition energy distribution to reconstruct the position. Three main situation which affect the deposition energy distribution are analyzed, and the influence of three situation on the deposition energy distribution is verified by experiments, finally the imaging accuracy of the scheme in the whole space was measured experimentally. The experiment proved that the reconstruction of ϕ mainly depends on situation 1), while the reconstruction of θ mainly depends on situations 2) and 3). Among them, situation 1) is the most sensitive to the position of the radiation source, thus achieving high reconstruction accuracy for ϕ across the entire space. The reconstruction of θ can be very accurate when situation 3) is dominant; if situation 2) is dominant, the reconstruction result is poor. In the future, it is possible to use multiple detector combinations or rotate detectors for multiple measurements to obtain high-precision ϕ and theta at the same time.

In this work, a new gamma camera was developed, and the most advanced and technologically mature similar imaging device on the market is the Compton camera [24–26]. The new gamma camera developed this time perfectly inherits the advantages of the Compton camera, but also has the advantages that the Compton camera does not have.

The advantages of inheritance include: 1. No collimator is required. Like the Compton camera, the equipment developed this time does not require a collimator at all, and truly achieves 4π field of view imaging. 2. High imaging sensitivity. Ideally, a Compton camera can reconstruct a hot spot location with very small number of events [27], but these events need to meet certain conditions, including the scattering in the scattering detector needs to be a single scatter, the absorption of all remaining energy deposited in the detector, and the photoelectric effect has only occurred. This kind of event does not account for a high proportion in the actual detection process, and it is necessary to select from all events or use multiple scattering events for reconstruction, resulting in a decrease in reconstruction sensitivity. The sensitivity can be done by the current advanced Compton camera < 30 nGy/h[28]. The radioactive source used in this test is Cs-137 (2 μCi, 30 cm away from the detector), and the sensitivity is about 60 nGy/h, which is similar to the performance of a Compton camera. 3. High reconstruction accuracy. The most advanced Compton camera currently available is the Compton Telescope SCoTSS based on semiconductor detectors [29, 30], achieving a localization precision of better than 2°, a standard deviation angular resolution of 2.8°–4.7°, or 6.6°–11.1° in FWHM. Such a design confines the sensitive FOV to be in front of the scatter detector layer, and thus is less than 4π. The ϕ reconstruction accuracy of the equipment developed in this study is less than 2.5°, and high-precision ϕ and θ can be obtained simultaneously using the method of joint imaging of multiple devices.

Compared with Compton cameras, the unique advantages of this development equipment. 1. Low cost. Compton cameras need to know the location, deposition energy, and timing of at least two photon interactions, which places high demands on the detector's time-resolved, energy-resolved, and readout electronics. As a result, advanced Compton cameras generally use semiconductor detection, but semiconductor detectors are expensive and require harsh operating conditions, making them unsuitable for commercial use [31]. Scintillator-based Compton cameras have also made great progress in recent years [32, 33], but the energy resolution of scintillator detectors is not as good as that of semiconductor detectors, resulting in much worse imaging accuracy than Compton cameras for semiconductor detectors, and some are even inferior to coding board imaging devices. However, the new equipment developed this time does not have high requirements for energy resolution and time resolution, and common detectors such as CsI and NaI can meet the requirements [34, 35]. 2. Wide range of work areas. Compton scattering must occur for the Compton camera, so it has more advantages in the field of high-energy γ-ray imaging, and the new equipment developed this time can also have good performance in the low-energy part and has a wider working energy range. In practical applications, it is impossible to pre-

dict the types of radioactive sources in advance in densely populated places such as customs and shopping malls, and a wider range of energy response is conducive to timely detection of potential risks. It must be noted that although we have conducted a series of single-hotspot and multi-hotspot test experiments in the laboratory and achieved good experimental results, the actual scenario is much more complex than the laboratory environment. Therefore, more detailed researchse are needed if the technology is to be truly applied to real life.

VIII. CONCLUSION

In this work, a novel gamma camera based on the distribution of deposited energy is developed. The device does not need a collimator, has a 4π imaging field of view, has low requirements for detector crystal performance, and has a simple reconstruction algorithm, which is very suitable for commercial large-scale use. Experimental tests are carried out using the Cs-137 source, which can give high reconstruction accuracy for both single and multiple hot spots, and the reconstruction accuracy mainly depends on the number of accumulated events and the position of the hot spot relative to the detector. It is concluded that the proposed design can be applied to the monitoring of radioactive source hotspots in nuclear safety applications.

[1] Jacques Guizerix, Vitomir Markovic, Peter Airey. Radioisotopes and radiation technology in industry. Nuclear techniques for peaceful development. IAEA BULLETIN, 2/1987.

[2] Yue Yu , Shuangquan Liu, Zhiming Zhang et al. Far-Field 3-D Localization of Radioactive Hotspots via Four-Eyes Stereo Gamma Camera. Nuclear techniques for peaceful development. IEEE TRANSACTIONS ON NUCLEAR SCIENCE, VOL. 69, NO. 8, AUGUST 2022

[3] Ji Hu, Hongyu Li, Yanying Sui,et al. Current status and future perspective of radiopharmaceuticals in China. European Journal of Nuclear Medicine and Molecular Imaging (2022) 49:2514–2530. Doi:10.1007/s00259-021-05615-6.

[4] Xi-Yang Cui, Yu Liu, Changlun Wang et al. China's radiopharmaceuticals on expressway: 2014–2021 .Radiochimica Acta. doi:10.1515/ract-2021-1137

[5] DUAN X, CAO Z, ZHU H, et al. 68Ga-labeled ODAP-Urea-based PSMA agents in prostate cancer: First-in-human imaging of an optimized agent. European Journal of Nuclear Medicine and Molecular Imaging, 2022, 49(3): 1030-1040. doi: 10.1007/s00259-021-05486-x.

[6] XUE Yue, XU Guangduo. Development Status of Nuclear Technology Application Industry in China[J]. Journal of Isotopes, 2021, 34(2): 97-103. DOI: 10.7538/tws.2021.34.02.0097.

[7] Y. Shirakawa, T. Yamano, Y. Kobayashi, Remote sensing of nuclear accidents using a direction finding detector, 2009 35th Annual Conference of IEEE Industrial Electronics, 2009, pp. 1917-1922

[8] S. Shifeng, Z. Zhiming, S. Lei et al. Far field 3D localization of radioactive hot spots using a coded aperture camera, Applied Radiation and Isotopes, 107 (2016) 177-182.

[9] LIU Bin, Lv Huanwen, Xu Hu, et al. A novel coded aperture for γ-ray imaging based on compressed sensing. Nuclear Instruments and Methods in Physics Research Section A: Accelerators, Spectrometers, Detectors and Associated Equipment, 2022, 1021: 165959. Doi: 10.1016/j.nima.2021.165959.

[10] ZHU Yuefeng, ANDERSON S E, HE Zhong. Sub-pixel position sensing for pixelated, 3-D position sensitive, wide bandgap, semiconductor, gammaray detectors. IEEE transactions on nuclear science, 2011,58(3):1400-1409.

[11] Z. Yao, Y. Yuan, J. Wu et al., Rapid Compton camera imaging for source terms investigation in the nuclear decommissioning with a subset-driven origin ensemble algorithm. Radiat. Phys. Chem.197, 110133 (2022). https:// doi. org/ 10. 1016/j. radphyschem. 2022.110133

[12] J. Zhang, X. Liang, J. Cai et al., Prototype of an array SiPM-based scintillator Compton camera for radioactive materials detection. Radiat. Detect. Technol. 3(3), 17 (2019). https:// doi. org/ 10. 1007/s41605- 019- 0095-1

[13] Inc H. D. H100 Gamma-Ray Imaging Spectrometer[[EB/OL]. https://h3dgamma.com/H100Specs.pdf, 2022.2.3

[14] Shinichiro T., Atsushi H., Yuto I.,et al. A Portable Si/CdTe Compton Camera and its Applications to the Visualization of Radioactive Substances. Nuclear Instruments and Methods in Physics Research Section A: Accelerators, Spectrometers, Detectors and Associated Equipment, 2015,787:207-211.

[15] Xiaofeng G., Qingpei X., Dongfeng T.,et al. Simulation Study of the Backward-Scattering Effect in Compton Imager. Applied Radiation and Isotopes, 2017,124:93-99.

[16] Liu Y., Fu J., Li Y.,et al. Preliminary Results of a Compton Camera Based On a Single 3D Position-Sensitive CZT Detector. Nuclear Science and Techniques, 2018,29(10):145

[17] Song lin, Qi hao-tian, Zhu li-hua. Novel Prototype of a Compton Camera Based on a Monolithic GAGG Crystal.Nuclear Science and Techniques. doi: 10.12074/202412.00182(accepted)

[18] C. Papadimitropoulos, I. Kaissas, C. Potiriadis et al. Lambropoulos,Radioactive source localization by a two detector system, J Instrum, 10 (2015) C12022-C12022. DOI 10.1088/1748-0221/10/12/C12022

[19] C.G. Wahl, W.R. Kaye, W. Wang, F et al. The Polaris-H imaging spectrometer, Nuclear Instruments and Methods in Physics Research Section A: Accelerators,Spectrometers, Detectors and Associated Equipment, 784 (2015) 377-381. https://doi.org/10.1016/j.nima.2014.12.110

[20] K. Takeuchi, J. Kataoka, T. Nishiyama et al. "Stereo Compton cameras" for the 3-D localization of radioisotopes, Nuclear Instruments and Methods in Physics Research Section A: Accelerators,Spectrometers, Detectors and Associated Equipment, 765 (2014) 187-191. https://doi.org/10.1016/j.nima.2014.04.039

[21] R. Bugalho, A. Di Francesco, L. Ferramacho, et al. Experimental characterization of the TOFPET2 ASIC . Journal of Instrumentation, 2019, 14, P03029. DOI:10.1088/1748-0221/14/03/P03029

[22] Hao Cheng,Bao-Hua Sun,Li-Hua Zhu et al.Intrinsic background radiation of $LaBr_3$(Ce) detector via coincidence mea-

surements and simulations. Nuclear Science and Techniques . 2020 ,31 (10). doi:10.1007/s41365-020-00812-8

[23] Y. Shirakawa, T. Yamano, Y. Kobayashi, Remote sensing of nuclear accidents using a direction finding detector, 2009 35th Annual Conference of IEEE Industrial Electronics, 2009, pp. 1917-1922.

[24] Ming-Hao Dong, Zhi-Yang Yao,Yong-Shun Xiao. Development and preliminary results of a large-pixel two-layer LaBr3 Compton camera prototype. Nuclear Science and Techniques (2023) 34:121. Doi:10.1007/s41365-023-01273-5

[25] Shikaze Y., Shimazoe K. Improvement of Analysis Results From the GAGG Scintillator Compton Camera Operated On an Unmanned Helicopter by Selecting Stable Flight Conditions. Journal of Nuclear Science and Technology, 2022,59(1):44-54.

[26] Sato Y., Terasaka Y. Radiation Imaging Using an Integrated Radiation Imaging System Based On a Compact Compton Camera Under Unit 1/2 Exhaust Stack of Fukushima Daiichi Nuclear Power Station. Journal of Nuclear Science and Technology, 2021:1-11.

[27] Zhi-Yang Yao,Yong-Shun Xiao, Ji-Zhong Zhao. Dose reconstruction with Compton camera during proton therapy via subset-driven origin ensemble and double evolutionary algorithm. Nuclear Science and Techniques (2023) 34:59 https://doi.org/10.1007/s41365-023-01207-1.

[28] Qing Ye, Peng Fan, Rui Wang et al. A high sensitivity 4π view gamma imager with a monolithic 3D position-sensitive detector. Nuclear Inst. and Methods in Physics Research, A. S0168-9002(19)30638-2. Doi:10.1016/j.nima.2019.05.022.

[29] L. Sinclair, P. Saull, D. Hanna, H. Seywerd, A. MacLeod, P. Boyle, Silicon Photomultiplier-Based Compton Telescope for Safety and Security (SCoTSS), IEEE Transactions on Nuclear Science, 61 (2014)2745-2752.

[30] A.M.L. MacLeod, P.J. Boyle, D.S. Hanna, P.R.B. Saull, L.E. Sinclair, H.C.J. Seywerd, Development of a Compton imager based on bars of scintillator, Nuclear Instruments and Methods in Physics Research Section A: Accelerators, Spectrometers, Detectors and Associated Equipment, 767 (2014) 397-406.

[31] X. C. Zhao,X. P. Ouyang,Y. D . X u et al. Time response of Cd0.9Zn0.1Te crystals under transient and pulsed irradiation. AIP ADVANCES 2, 012162 (2012).

[32] R. Wu, C. Geng, F. Tian et al., GPU-accelerated three dimensional reconstruction method of the Compton camera and its application in radionuclide imaging. Nucl. Sci. Tech.34(4), 52 (2023). doi:org/ 10. 1007/ s41365- 023- 01199-y

[33] Z. Yao, Y. Xiao, B. Wang et al., Study of 3D fast Compton camera image reconstruction method by algebraic spatial sampling. Nucl. Instrum. Meth. A 954, 161345 (2018). doi: org/10. 1016/j.nima. 2018. 10. 023

[34] Shengling Huang, Xin Wang, Yifan Chen et al. Modeling and quantitative analysis of X-ray transmission and backscatter imaging aimed at security inspection.Opt. Express,2019,27(2):337-349 doi: 10.1364/OE.27.000337

[35] Zhi Yang 1, Tianchi Wang 2, Xuhui Xu et al.Fiber Optic Plate Coupled Pb-Free Perovskite X-ray Camera Featuring Low-Dose-Rate Imaging toward Dental Diagnosis.Phys. Chem. Lett.,2023,14(2): 326-333. DOI: 10.1021/acs.jpclett.2c03586